Steel and Composite Structures, *Vol. 36, No. 3 (2020) 261-272*
DOI: https://doi.org/10.12989/scs.2020.36.3.261

Shear behavior and shear capacity prediction of precast concrete-encased steel beams

Yunlong Yu[1,2], Yong Yang[1,2], Yicong Xue*[1] and Yaping Liu[3]

[1]School of Civil Engineering, Xi'an University of Architecture & Technology, Shaanxi, China
[2]Key Lab of Structural Engineering and Earthquake Resistance, Ministry of Education, China
[3]China Qiyuan Engineering Corporation, Shaanxi, China

(*Received February 4, 2020, Revised July 7, 2020, Accepted July 8, 2020*)

Abstract. A novel precast concrete-encased steel composite beam, which can be abbreviated as PCES beam, is introduced in this paper. In order to investigate the shear behavior of this PCES beam, a test of eight full-scale PCES beam specimens was carried out, in which the specimens were subjected to positive bending moment or negative bending moment, respectively. The factors which affected the shear behavior, such as the shear span-to-depth aspect ratio and the existence of concrete flange, were taken into account. During the test, the load-deflection curves of the test specimens were recorded, while the crack propagation patterns together with the failure patterns were observed as well. From the test results, it could be concluded that the tested PCES beams could all exhibit ductile shear behavior, and the innovative shear connectors between the precast concrete and cast-in-place concrete, namely the precast concrete transverse diaphragms, were verified to be effective. Then, based on the shear deformation compatibility, a theoretical model for predicting the shear capacity of the proposed PCES beams was put forward and verified to be valid with the good agreement of the shear capacities calculated using the proposed method and those from the experiments. Finally, in order to facilitate the preliminary design in practical applications, a simplified calculation method for predicting the shear capacity of the proposed PCES beams was also put forward and validated using available test results.

Keywords: Precast concrete-encased steel beam; shear capacity; hogging bending moment; sagging bending moment; experimental study; truss-arch model

1. Introduction

Concrete-encased steel (CES) structures, in which structural member is usually composed of a steel shape and a reinforced concrete part, are well known in structural engineering due to the outstanding mechanical performance, good fire resistance as well as good durability ability. Nevertheless, traditional CES structures sometimes cannot be the first choice of structure designers because of the shortcomings of relatively complex process and high cost during the construction period (Zhu *et al.* 2017, Lacki *et al.* 2018, Chen and Liu 2018, Yan *et al.* 2019, Yang *et al.* 2019a, Yang *et al.* 2019b, Lai *et al.* 2019, Li *et al.* 2019, Du *et al.* 2019, Thusoo *et al.* 2020). The construction process of a traditional CES structure could be separated into at least four main steps as steel shape locating, reinforcement skeleton assembling, formwork installing, and concrete casting. All these four steps are usually conducted on construction site, which leads to more cost in labor force and longer construction period than steel structures and traditional reinforced concrete structures.

In order to facilitate the steel-concrete composite construction, some researchers have examined the benefits of combining precast concrete and steel-concrete composite structures. For example, Patel *et al.* (2018) proposed a novel demountable composite beam, which could be assembled using bolts and demountable nuts.

Similarly, in order to overcome the complex on-site construction of traditional CES structures, an innovative beam construction method, namely, the precast concrete-encased steel (PCES) structure, is proposed in this paper. In the PCES structure, structural members such as columns and beams can be constructed separately in two steps. The first step is conducted in precast factory, and the second step is conducted on construction site after the precast part transported, lifted and set up. Because the deadweight of the precast part of PCES beams could be much smaller than that of the entirely precast CES beam, it does not need any special vehicle or crane to transport and lift. For the cast-in-place part, the inner concrete can be cast and cured together with the adjacent floor slab to enhance the structural integrity. In order to explore the mechanical behavior of PCES beams, Hong *et al.* (2009, 2010a, b, c) have conducted a series of experiments to investigate the flexural behavior of PCES beams, but the shear behavior of PCES beams was rarely reported. Meanwhile, the special construction method to transfer the longitudinal shear stress between the precast part and the cast-in-place part is limited in the PCES beams proposed by Hong *et al*, indicating that debonding might occur.

A novel PCES beam is presented in this paper. The construction process of the proposed PCES beam is illustrated in Fig. 1. As shown in Fig. 1, this innovative

*Corresponding author, Associate Professor
E-mail: xjdxyc@foxmail.com

ISSN: 1229-9367 (Print), 1598-6233 (Online)

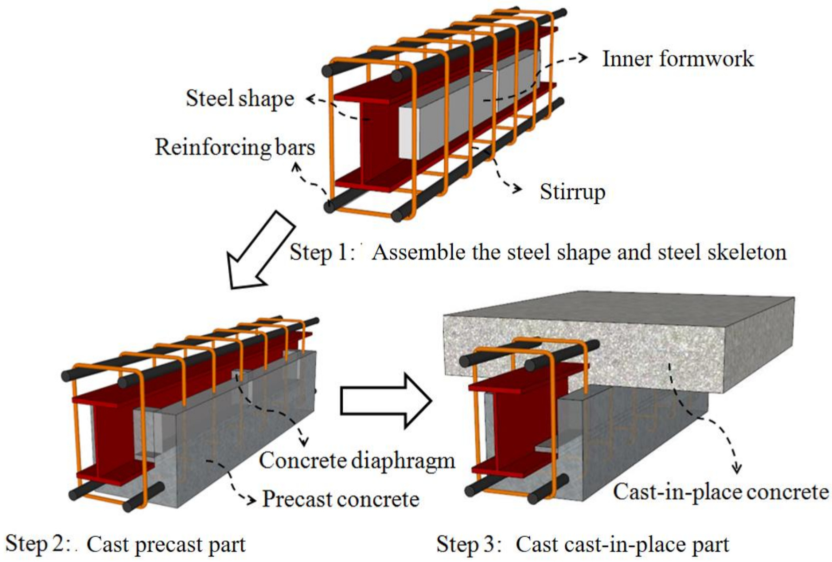

Fig. 1 Schematic diagram of proposed PCES beam

PCES beam is also composed of a precast outer-part and a cast-in-place inner-part. In order to enhance the bonding behavior between the precast concrete, cast-in-place concrete and steel shape, in the outer part, a series of concrete diaphragms are designed to resist the longitudinal shear force on the interface. These transverse diaphragms can be regarded as large shear connectors to transfer the longitudinal shear stress and to make sure that no slippage occurs on the interface.

Different from the PCES beam which is invented by Hong *et al.* (2009, 2010a, b, c), in the proposed PCES beam, two different concrete materials are designed in the beam cross-section, which also makes the PCES beam different from traditional CES beams. The precast U-shape shell with transverse diaphragms is cast using high-strength concrete to enhance the stiffness during the on-site construction process, which can reduce the vertical deflection at the mid-span and cut the cost of external braces. Meanwhile, the cast-in-place part can be cast using conventional concrete to save the expensive high-strength concrete. Therefore, the advantages of the traditional CES beam, such as the outstanding mechanical performance and fire resistance, can still be found in the proposed PCES beam, which is superior in construction ability and section diversity to the traditional CES beam.

Nevertheless, the difference in concrete strength between the precast part and the cast-in-place part is supposed to affect the mechanical behavior of the proposed PCES beam obviously, especially in its shear performance. Therefore, experimental and theoretical research are necessary to investigate the shear performance to establish new design methods of this proposed PCES beam.

2. Test program

2.1 Test specimens

Eight specimens were designed in this experiment, and all the key parameters regarding the test specimens were listed in the Table 1. These eight PCES beams included six T-beams and two rectangular beams, indicating that six test-pieces were designed with concrete flange, which could simulate the adjacent floor slab. According to the bending moment which the specimens were supposed to bear, these eight specimens were sorted into three categories namely, series A, series B in which specimens were under sagging moment and series C in which specimens were under hogging moment. For the five specimens of series A and series B, the main target was to explore the shear performance of PCES beams under sagging moment, so the concrete flange of these specimens was supposed to be in compression zone. For the three specimens of series C, they aimed to be tested under hogging moment, so the concrete flanges were supposed to be in tension zone.

2.2 Cross sections

The test specimens have two different cross section forms. As shown in Fig. 2, all information of the section details, longitudinal and transverse reinforcements of the test specimens could be found below:

The height and the width of the specimen web core were both 450 mm, and the width and the thickness of the concrete flange were 880 mm and 200 mm. The steel shape in all the specimens was HN500×200×9×14 per the Chinese standards, indicating that the total width and height of the applied steel shape were 200 mm and 500 mm, and the thicknesses of the steel flange and web were 14 mm and 9 mm, respectively. The specimens in series A are designed with rectangle section to explore the shear behavior of PCES beams which are applied in the structures without slab, such as factory and theatre.

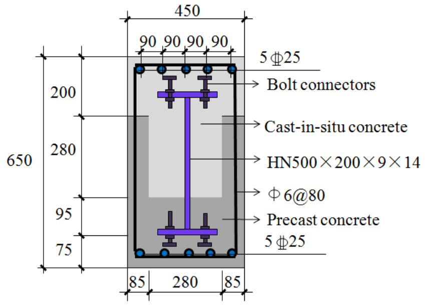

(a) Series A

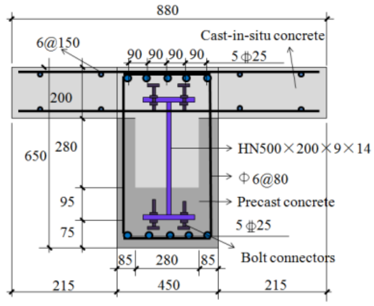

(b) Series B and Series C

Fig. 2 Design details

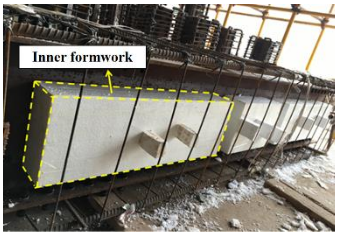

(a) Before outer-part cast

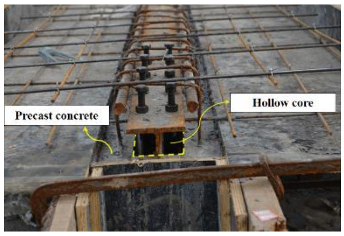

(b) After outer-part cast

Fig. 3 Construction of PCES beams

Table 1 Design parameters of test specimens

Series No.	Specimen ID	h_0 (mm)	L_0 (mm)	a (mm)	l (mm)	l/h_0	$f_{cu,out}$ (MPa)	$f_{cu,in}$ (MPa)
A	PCES-1-1	610	2300	600	610	1.0	45.0	31.8
	PCES-1-2		2700	600	915	1.5		
B	PCES-2-1		1600	600	305	0.5		
	PCES-2-2		2300	600	610	1.0		
	PCES-2-3		2700	600	915	1.5		
C	PCES-3-1		1600	600	305	0.5		
	PCES-3-2		2300	600	610	1.0		
	PCES-3-3		2700	600	915	1.5		

Note: L_0 is the specimen length; h_0 is the effective depth, which can be determined as the distance from the beam top to the center of tensile longitudinal rebar; a is the distance between the two loading points; l is the shear span length; $f_{cu,out}$ is the cubic strength of the outer-part concrete; $f_{cu,in}$ is the cubic strength of the inner-part concrete.

2.3 Construction procedure

As denoted in Fig. 3, all the PCES specimens were constructed in two steps. The first step was the precast step. As mentioned above and highlighted in dark gray in Fig. 2, the precast outer-part consisted of a H-steel shape, high-strength concrete, longitudinal and transverse reinforcements and concrete diaphragm plates. The steel shape, longitudinal reinforcements and stirrups were fabricated in precast factory, and foam formwork was attached at the both sides of the steel web. The transverse concrete diaphragms formed when the precast concrete flowed into the gap between two foam cubes, and the outer-part of the specimens was cast and cured at the same conditions using high-strength concrete. In the second step, the inner-part of the specimens, which was composed of the beam web core and the beam flange, was cast in this step using conventional concrete. During this step, no formwork and shoring work was needed.

Table 2 Material properties

Material		Grade	Diameter (mm)	Thickness (mm)	Width (mm)	E_s (MPa)	f_y (MPa)	f_u (MPa)
Steel shape	Flange	Q235B	-	9	500	2.05×10^5	273	450
	Web	Q235B		14	200	2.05×10^5	262	436
Steel bolts		10.9	16	-	-	-	960*	1215*
Steel rebar		HPB300	6	-	-	2.00×10^5	387	545
		HRB400	18	-	-	2.00×10^5	420	578
		HRB400	25	-	-	2.00×10^5	443	598

Note: E_s is the modulus of elasticity; and f_y is the yield strength; f_u is the ultimate strength; "*" denotes that the data which i s provided by the manufacturer.

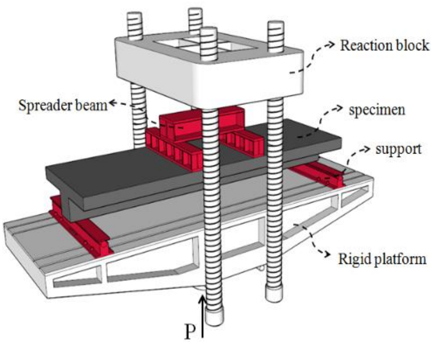

(a) Electro hydraulic servo-testing machine

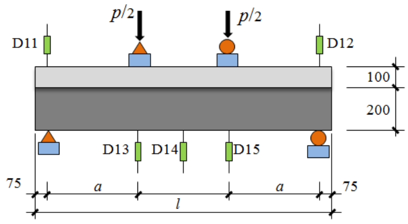

(b) Layout of LVDTs

Fig. 4 Schematic diagram of test setup

The precast part and the cast-in-place part were connected using concrete diaphragms and high-strength bolts. The steel bolts were fixed at the steel flanges by two steel nuts, therefore, the bolt head was in the precast concrete and its rear was in the cast-in-place concrete, indicating that the bolt connectors could coordinate the deformation between the steel shape, precast concrete and cast-in-place concrete.

2.4 Materials

For all the PCES specimens, the tested cubic compressive strength of concrete in the outer-part was 45.0 MPa, and that in the inner-part was 31.8 MPa. The detailed material properties of applied concrete were recorded in Table 1.

For the steel shape, the tested tensile strength of the steel flange was 273 MPa at yield and 450 MPa at peak, respectively; the tested tensile strength of the steel web was 262 MPa at yield and 436 MPa at peak, respectively. For the rebar reinforcements, the tested tensile strength of the stirrups, namely the rebar with a diameter of 6 mm, was 387 MPa at yield and 545 MPa at peak, respectively; the tested tensile strength of the longitudinal reinforcements, namely the rebar with a diameter of 18 mm, was 420 MPa at yield and 578 MPa at peak, respectively; the tested tensile strength of the rebar with a diameter of 25 mm, was 443 MPa at yield and 598 MPa at peak, respectively. For the shear connectors, the steel bolts with the grade of 10.9 per the Chinese codes were applied, and the yield and ultimate strengths, which were all provided by the manufacturer, were 960 MPa and 1215 MPa, respectively. The detailed mechanical properties of the steel reinforcements could be found in Table 2.

2.5 Test device

The specimens were tested on a compression machine with the maximum capacity of 20000 kN, which was illustrated in Fig. 4. As shown in Fig. 4, the concrete flange of the specimens in series B, which were designed to subject sagging moment, was placed upward and supposed to work in the compression zone. Meanwhile, the concrete flange of the specimens in series C, which were designed to subject hogging moment, was placed downward and supposed to work in the tension zone. In order to study the effect of shear span-to-depth ratios on the shear performance of the test PCES beams, the total length of the test specimens was different, and the length distance between the two loading points was fixed, indicating that the shear spans of the specimens could be adjusted to stimulate different shear span-to-depth ratios. The layout of LVDTs was presented in Fig. 4(b) in detail, and the layout of strain gauges was illustrated in Fig. 5.

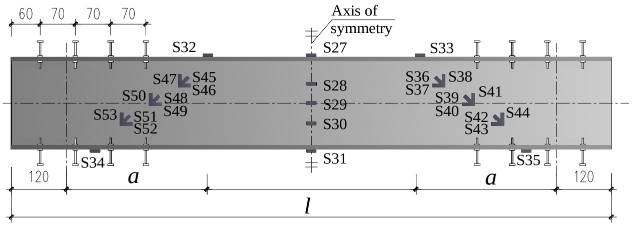

(a) Steel shape

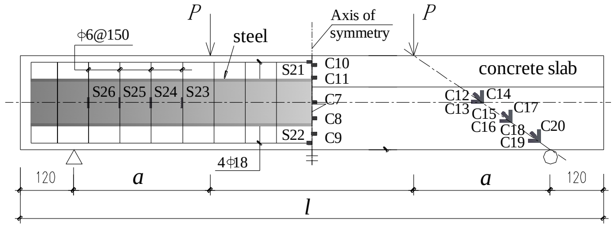

(b) Concrete and stirrups

Fig. 5 Schematic diagram of strain gauge arrangement (Unit: mm)

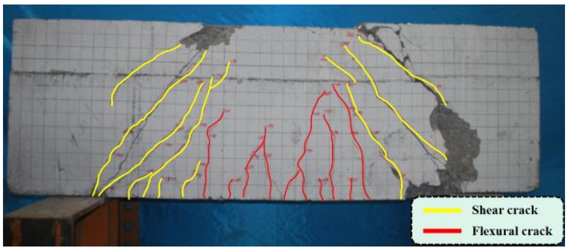

(a) PCES-1-1

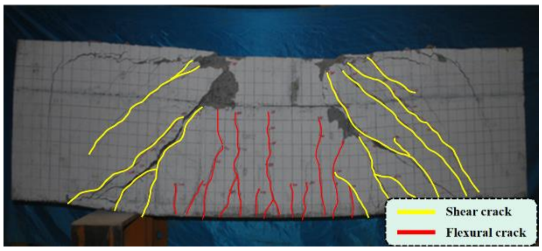

(b) PCES-1-2

Fig. 6 Failure modes of specimens in series A

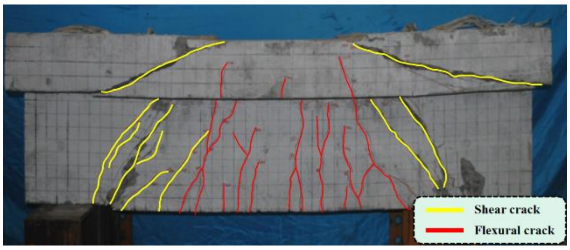

(a) PCES-2-1

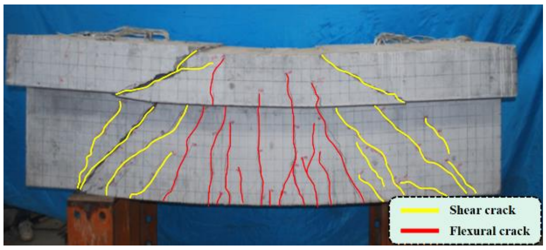

(b) PCES-2-2

Fig. 7 Failure modes of specimens in series B

3. Test results

3.1 Crack patterns and failure modes

The crack patterns and failure modes of the typical specimens in series A to series C were shown in Fig. 6, Figs. 7 and 8, respectively. As illustrated in these figures, all the specimens failed in typical shear compression failure mode. For the specimens in series A and series B, a series of flexural cracks occurred firstly at the shear span in the tension zone of the cross section, and then a series of inclined cracks, namely the flexural-shear cracks, developed shortly afterward. With the increasing of the applied load, a longitudinal crack along with many tiny cracks occurred on the top surface of the concrete flange, which caused a fast development of the vertical deflection together with a slow decreasing of the applied load. Finally, with the propagation of the inclined cracks and the longitudinal cracks in the two shear spans, the top concrete crushed, which caused the final failure. The longitudinal crack on the top surface of the concrete flange might be caused by the different flexural stiffness between the reinforced concrete part and the steel shape. Because the longitudinal crack was not observed on the lateral side of the specimens, the bonding between the concrete and the steel shape could still be concrete.

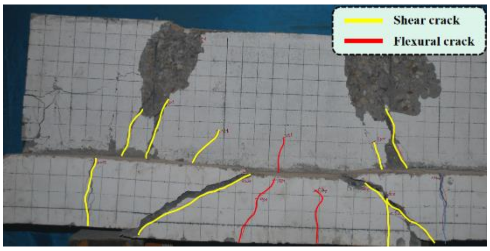

(a) PCES-3-1

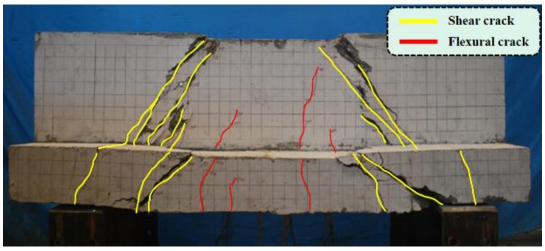

(b) PCES-3-2

Fig. 8 Failure modes of specimens in series C

For the specimens in series C, the failure modes were similar to those of the specimens in series B, except for the cracking propagation because of the different position of the concrete flange. In these specimens, some transverse cracks initiated from the bottom surface of the concrete flange which located at the tension zone. Then, these cracks propagated to the web of the specimens and formed a series of inclined cracks. Finally, these specimens failed due to the concrete crushing. Because the concrete flange cracked at the beginning of the test, it indicated that the concrete flange of the specimens in series C could not provide any additional shear capacity when compared with the specimens in series B.

For all the test specimens, the flexural cracks, which could be observed between the two loading points and highlighted in red in Figs. 6-8, were effectively restrained without stretching to the beam top. Meanwhile, the shear cracks, which could be observed between the support and the loading point and highlighted in yellow, propagated thorough the beam height, indicating that the test specimens all suffered the shear failure and hardly affected by flexure.

As can be observed from the test phenomenon, the inclination of the critical shear crack band of all the specimens was found from the line joining the centers of the support and the loading point, indicating that not all of the shear cracks experienced a fixed angle of 45-degree. Therefore, the traditional truss analogy, in which the inclination of the horizontal chord and the diagonal chord is assumed as 45-degree, should be revised in the shear strength prediction. During the test process, there was not any visible slippage found on the interface between the concrete and steel shape in all the test specimens, indicating that these two parts bonded to each other well. Therefore, from the test results and observations, it could be concluded that the mechanical performance such as the member integrity and composite action were good enough as expected, and the shear connectors, namely the transverse concrete diaphragms and bolt connectors, effectively transfer the longitudinal stress on the interface.

3.2 Load-deflection curves

Fig. 9 shows the load-deflection curves of the test specimens. From the load-deflection curves of the specimens in series A, it could be found that all the specimens behaved in a ductile manner, even for the specimen PCES-1-1 whose shear span-to-depth ratio was 1.0. Meanwhile, it could be also observed that there was no obvious difference between all the specimens in series B and series C in initial stiffness, except for the specimens in series A. It indicated that the initial stiffness of the PCES beams with a rectangle section increased with the decrease of the aspect ratio, but the existence of the concrete flange could narrow the gap.

Compared with the load-deflection curves of the specimens in series A, although there was a mild drop of the applied load after the peak-load point reached, specimens PCES-2-1, PCES-2-2 and PCES-2-3 could still avoid the sharp drop in load during the post-peak load period, which denoted that the final failure was ductile. The shear behavior of the specimens in series C was similar to that of the specimens in series B, but the peak load of the specimens in series C was a bit lower, indicating that the existence of the concrete flange could enhance the shear capacity of the test PCES beams.

4. Discussions on shear capacity

The measured shear capacities of the test specimens were listed in Table 3, and the effects of different design parameters on the shear capacity were discussed as follows in this section.

4.1 Effect of concrete flange

As mentioned before, there were some differences between the failure modes of the specimens in series B and those in series C, which could be mainly observed in the cracking propagation process due to the position of the concrete flange. For the specimens in series B, which were subjected to sagging moment, the concrete flange of the specimens was placed in the compression zone and longitudinally cracked due to the compression force, and then crushed at the end of the test. It meant that the concrete flange did bear some part of the compression force at the shear-compression zone and could contribute some shear capacity to the entire beam. However, for the specimens in series C, which were subjected to hogging moment, the concrete flange was located in the tension zone and transversely cracked at the beginning of the test, and then seriously cracked shortly. It meant that the concrete flange

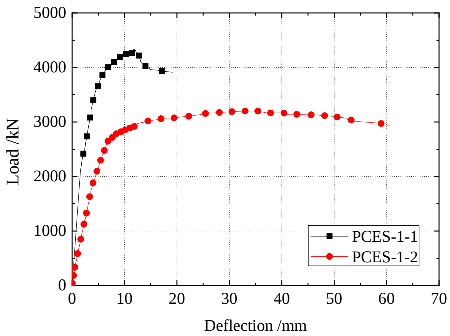

(a) Specimens in series A

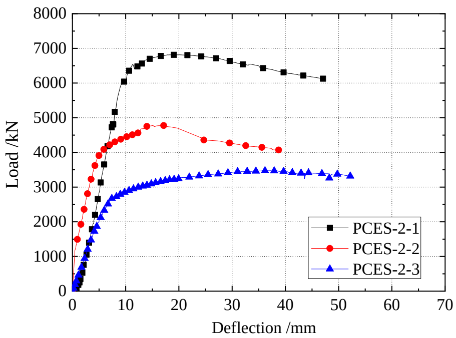

(b) Specimens in series B

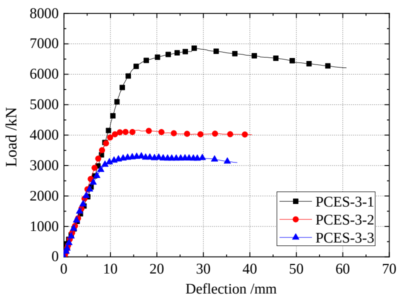

(c) Specimens in series C

Fig. 9 Load-deflection curves

of the specimens in series C could not play an important role in the shear performance. As recorded in Table 3, it could be also found that the shear capacity of the specimens subjected to sagging moment was higher than that of the specimens subjected to hogging moment, despite all the cross sectional dimensions and the material parameters were all the same.

As shown in Fig. 10, the difference in percentage of the shear capacities between the specimens subjected to hogging moment and the specimens subjected to sagging moment ranged from 1.5% to 15%. Therefore, the existence of the concrete flange on the shear behavior should be considered. A previous research conducted by Placasal and Regan (1971) reported that the shear capacity of flanged RC beams increased with the increasing of the ratio of flange width to beam width, and a stable increase of 20% could be observed when the ratio of flange width to beam width was over 2.0. Additionally, the previous numerical analysis conducted by the authors also demonstrated that the existence of the concrete flange could enhance the shear

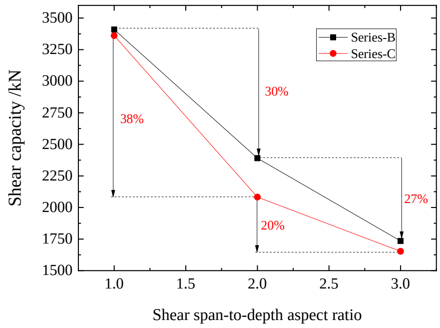

Fig. 11 Effect of shear span-to-depth ratio

capacity of the traditional T-shape CES beams, and an increase of approximately 15% in shear capacity could be observed when the ratio of flange width to beam width was 2.0 and the shear span-to-depth ratio was 1.5 (Yu 2017).

4.2 Effect of shear span-to-depth ratio

Shear spacing directly affected the peak loads of the tested PCES beams, because the arch action and truss action, which were the two major mechanisms existed in structural members, were all sensitive to the length of the shear span. The arch action, which could lead to a higher stiffness and strength than the truss action, was striking when the shear span was small, and the truss action, which could lead to a better deformability than the arch action, was dominant when the shear span was long. Fig. 11 shows the relationships between the shear span-to-depth ratio and the shear capacity of the specimens. It could be observed that the shear capacity of the specimens was highly affected by the shear span-to-depth ratio. For instance, the shear capacities of specimens PCES-2-1, PCES-2-2 and PCES-2-3, which were identical in all of the dimensions and material parameters, were 3409 kN, 2390 kN and 1735 kN with the shear span-to-depth ratios of 0.5, 1.0 and 1.5 respectively, and the shear capacities of specimens PCES-3-1, PCES-3-2 and PCES-3-3 followed the same trend. From the results above, it revealed that the shear capacity of the PCES beams decreased proportionally with the increasing of the shear span-to-depth ratio.

5. Calculation methods of shear capacity

5.1 Compatible truss-arch model

A set of formulas were proposed to predict the shear capacity of the PCES beams, and the shear capacity of a PCES beam consisting of three parts is expressed as follows

$$V = V_t + V_a + V_{ss} \tag{1}$$

where $V_t = V_s + V_c$, V_s and V_c are the contributions of the transverse reinforcements and concrete to the shear capacity of the truss model, respectively; V_{ss} is the shear capacity provided by the steel shape; V_a is the shear capacity provided by the arch action.

Table 3 Test results

Series No.	Specimen ID	Load of the first flexural crack	Load of the first inclined crack	Peak load P_u/kN	Shear capacity V_u/kN	V_{JGJ}/V_u	V_{YB}/V_u	V_{sim}/V_u	V_{com}/V_u
A	PCES-1-1	470	650	4340	2170	0.72	0.99	0.76	0.94
	PCES-1-2	320	600	3200	1600	0.74	1.26	0.94	0.98
B	PCES-2-1	600	820	6817	3409	0.75	0.69	0.63	0.97
	PCES-2-2	680	640	4780	2390	0.66	0.89	0.76	1.14
	PCES-2-3	500	630	3470	1735	0.68	1.16	0.95	1.18
C	PCES-3-1	1150	1000	6721	3361	0.76	0.70	0.56	0.83
	PCES-3-2	450	700	4164	2082	0.76	1.03	0.79	1.09
	PCES-3-3	500	1000	3306	1653	0.72	1.22	0.91	1.03
Yu (2018)	PPSRC-1	180	320	1324	662	0.45	0.58	0.73	0.84
	PPSRC-2	100	220	919	460	0.50	0.78	0.91	0.92
	PPSRC-3	94	120	784	392	0.52	0.88	1.00	0.94
	PPSRC-4	94	160	887	444	0.44	0.73	0.81	0.92
	PPSRC-5	120	330	988	494	0.53	0.79	1.01	0.89
	SRC-1	180	260	1030	515	0.55	0.80	1.00	0.85
	PPSRC-16	307	205	1024	512	0.58	0.76	0.91	0.88
	PPSRC-17	172	195	750	375	0.62	0.96	0.63	0.91
	PPSRC-18	136	236	620	310	0.66	1.12	0.77	0.94
	PPSRC-19	133	152	632	316	0.62	1.03	0.90	0.99
	PPSRC-20	189	291	786	393	0.66	0.99	0.86	1.09
	SRC-2	176	267	764	382	0.74	1.08	0.81	0.93
		Mean				0.63	0.92	0.83	0.96
		Coefficient of variation				0.16	0.20	0.15	0.10

Note: V_{JGJ} is the calculated shear capacity using the code JGJ 138-2016; V_{JGJ} is the calculated shear capacity using the code YB 9082-2006; V_{sim} is the calculated shear capacity using the simplified calculation method; V_{com} is the calculated shear capacity using the proposed model

The contributions of the transverse reinforcement and concrete to the shear capacity of the truss model are based on the simplified modified compression field theory (Bentz *et al*. 2006). The contribution of the transverse reinforcement to the shear capacity can be expressed as

$$V_s = \frac{A_{sv} f_{yv} h_0}{s} \cot\theta \tag{2}$$

where A_{sv} is the cross-sectional area of stirrups; f_{yv} is the yield strength of stirrups; s is the spacing of stirrups; θ is the angle of the inclined concrete strut with respect to longitudinal axis of the beam.

The concrete contribution to the shear capacity of the truss model, V_c, is expressed as

$$V_c = \beta b h_0 \sqrt{f_c} \tag{3}$$

where b is the width of the beam section; f_c is the compressive strength of applied concrete; β is a strength factor, which can be determined later in this section.

For the PCES beams proposed in this paper, there are two kinds of concrete in the cross section, so the combined properties of these two kinds of concrete were used. The composite concrete strength and composite modulus of elasticity could be calculated by Eqs. (4) and (5).

$$f_{c,com} = \frac{A_{c1}}{A_{c1}+A_{c2}} f_{c1} + \frac{A_{c2}}{A_{c1}+A_{c2}} f_{c2} \tag{4}$$

$$E_{c,com}=\frac{A_{c1}}{A_{c1}+A_{c2}}E_{c1}+\frac{A_{c2}}{A_{c1}+A_{c2}}E_{c2} \tag{5}$$

where A_{c1}, A_{c2} are the areas of the cast-in-place concrete and precast concrete in the rectangular-section beam; f_{c1}, f_{c2} are the compressive strengths of the cast-in-place concrete and precast concrete; E_{c1}, E_{c2} are the modulus of elasticity of the cast-in-place concrete and precast concrete.

Bentz *et al*. (2006) proposed a simplified method to calculate the value of β:

$$\beta=\frac{0.40}{1+1500\varepsilon_x}\times\frac{1300}{1000+\varepsilon_{ze}} \tag{6}$$

where ε_{ze} can be simply taken as 300 mm; ε_x is the longitudinal strain at the mid-depth of the cross section. ε_x can be computed by Eq. (7), which was proposed by Collins *et al*. (1996)

$$\varepsilon_x=\frac{\frac{V_t l}{d}+0.5V_t\cot\theta}{2E_sA_s} \tag{7}$$

where l is the length of the shear span; d is the distance between the tensile and compressive rebar; E_s is the modulus of elasticity of rebar; A_s is the gross cross-sectional area of tensile rebar. As proposed by Kim and Mander (2007), the expression for θ can be expressed as follows:

$$\theta=\arctan\left(\frac{0.6\rho_v n+0.57\frac{\rho_v A_v}{A_s}}{1+4n\rho_v}\right)^{0.25} \tag{8}$$

where n is obtained by the modulus of elasticity of steel dividing by that of concrete; ρ_v is the stirrup ratio; A_v is the area enclosed by stirrup.

The contributions of the compressive arch and steel shape to the overall shear capacity can be determined from the deformation compatibility between the truss and the concrete arch. The expression for the compatible condition is expressed as

$$\gamma=\frac{V_t}{K_t}=\frac{V_a}{K_a}=\frac{V_{ss}}{K_{ss}} \tag{9}$$

where γ is the shear deformation; K_a, K_t and K_{ss} are the shear stiffness of the arch, truss and steel shape, respectively; V_a, V_t and V_{ss} are the shear strengths of the arch, truss and steel shape, respectively.

As shown in Figs. 12 and 13, Pan and Li (2013) deduced the shear stiffness of the truss model and that of the arch model, which can be expressed as follows

$$K_t=\frac{V_t}{\frac{\delta_s+\delta_c}{d\cot\theta}}=\frac{V_t}{\frac{V_t}{E_cbd\sin^2\theta\cos^2\theta}+\frac{V_t}{E_s\rho_v b\cot^2\theta}}=\frac{n\rho_v E_cbd\cot^2\theta}{1+n\rho_v\csc^4\theta} \tag{10}$$

$$K_a=\frac{V_a}{\gamma_a}=\frac{V_a}{\frac{\delta_a}{l}}=E_cbc_a\cos^2\alpha\sin^2\alpha \tag{11}$$

where α is the angle of the concrete arch with respect to longitudinal axis of the beam.

The depth of the compressive arch is $c_a\cos\alpha$, where c_a is the effective depth of the compressive strut in the arch action. Based on the section analysis and regression analysis, a simplified method for calculating c_a was proposed as Eq. (12), which was proposed by Choi and Hong (2007)

$$c_a=(1-0.43\lambda)\cdot\left[\frac{3d\sqrt{(E_s\varepsilon_{c0}\rho_s)^2+\frac{4}{3}E_s\varepsilon_{c0}\rho_s(2+0.44\lambda)f_{c,com}}-3dE_s\varepsilon_{c0}\rho_s}{2(2+0.44\lambda)f_{c,com}}\right] \tag{12}$$

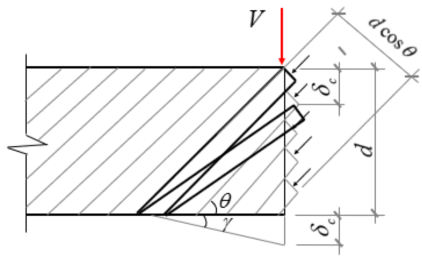

(a) Diagonal strut of concrete

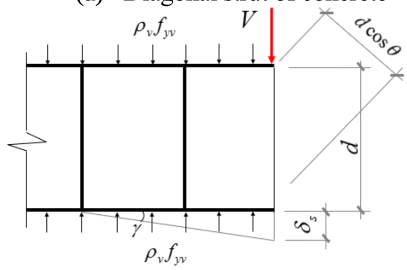

(b) Reinforcement skeleton

Fig. 12 Shear deformation of truss model

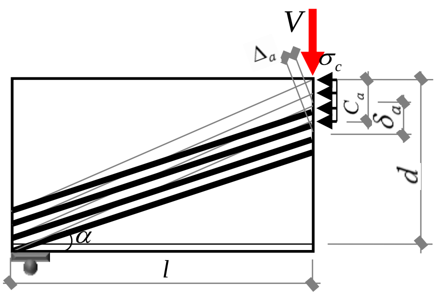

Fig. 13 Shear deformation of arch model

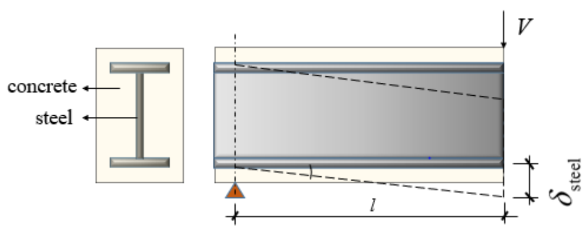

Fig. 14 Shear deformation of steel shape

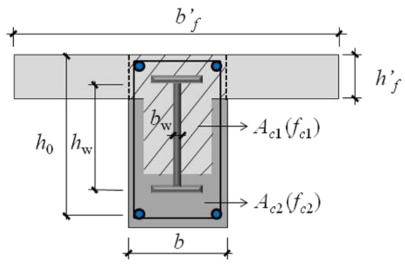

Fig. 15 Calculation diagram of simplified method

where λ is the shear span-to-depth ratio; ε_{c0} is the peak compressive strain of concrete, ε_{c0}=0.002; ρ_s is the reinforcement ratio of tensile rebar.

The calculation diagram of the shear capacity and shear stiffness of the steel shape are shown in Fig. 14, and the shear capacity of the steel shape can be determined by Eq. (13)

$$V_{ss} = V_t \frac{K_{ss}}{K_t} \tag{13}$$

The vertical deformation of the steel shape under shear can be obtained by diagram multiplication method in structural mechanics.

$$\delta_{steel} = \sum \int \overline{Q}_k d\upsilon_P = \sum \frac{\overline{Q}_k Q_P}{GA} = \frac{V_{ss} l}{GA} \tag{14}$$

where G is the shear modulus of steel shape; A is the cross-sectional area of steel web.

The shear stiffness of the steel shape can be determined as

$$K_{ss} = \frac{V_{ss}}{\gamma} = \frac{V_{ss}}{\frac{\delta_{steel}}{l}} = GA \tag{15}$$

Therefore, the shear capacity of the PCES beam can be calculated as

$$V_{com} = \mu(V_t + V_a + V_{ss}) = \mu V_t (1 + \frac{K_a}{K_t} + \frac{K_{ss}}{K_t}) \tag{16}$$

where μ is a coefficient which takes the effect of the concrete flange on the shear capacity of the specimens into account. Placasal and Regan (1971) suggested that μ=1.20 when $b_f^{'}/b \geq 2$.

5.2 Simplified method

Based on the existing specifications of steel and concrete composite structures, a simplified method for predicting the shear capacity of the PCES beams is proposed here as Eqs. (17)-(19), and the calculation diagram is shown in Fig. 15.

$$V_{sim} = \frac{1.75\left(\gamma_f^{'} + 1.0\right)}{\lambda + 1.0} f_{t,com} b h_0 + \frac{h_w t_w f_{ys}}{\sqrt{3}} + \frac{f_{yv} A_{sv}}{s} h_0 \tag{17}$$

$$f_{t,com} = \frac{A_{c1}}{A_{c1} + A_{c2}} f_{t1} + \frac{A_{c2}}{A_{c1} + A_{c2}} f_{t2} \tag{18}$$

$$\gamma_f^{'} = \frac{\left(b_f^{'} - b\right) h_f^{'} f_{t1}}{A_{c1} f_{t1} + A_{c2} f_{t2}} \tag{19}$$

where $f_{t,com}$ is the composite tensile strength of concrete part; t_w is the thickness of the steel shape web; h_w is the height of the steel shape web; f_{ys} is the yield strength of the steel shape; γ_f' is a coefficient which takes the effect of concrete flange on the shear capacity into account.

Table 3 listed the ratio of measured to calculated shear capacity using the proposed model, simplified model and calculation models from the codes JGJ 138-2016 and YB 9082-2006, of which the calculation formulas are recorded in Eqs. (20) and (21).

$$V_{JGJ} = \frac{1.75}{\lambda + 1.0} f_{t,com} b h_{0\text{-JGJ}} + \frac{0.58 h_w t_w f_{ys}}{\lambda} + \frac{f_{yv} A_{sv}}{s} h_{0\text{-JGJ}} \tag{20}$$

$$V_{YB} = \frac{1.75}{\lambda + 1.0} f_{t,com} b h_0 + \frac{h_w t_w f_{ys}}{\sqrt{3}} + \frac{f_{yv} A_{sv}}{s} h_0 \tag{21}$$

where $h_{0\text{-JGJ}}$ is the distance from the beam top to the resultant of the tensile longitudinal rebar and tensile steel flange.

Meanwhile, the test results of small-scale precast steel reinforced concrete beams, whose section arrangement was similar to the proposed PCES beam in this paper, were also cited here to validate the proposed calculation method. The mean ratios of measured to calculated shear capacity and values of coefficient of variation are 0.96 and 0.10, 0.83 and 0.15, 0.63 and 0.16, 0.92 and 0.20, for the proposed model, simplified model and models from JGJ 138-2016 and YB 9082-2006, respectively. The results indicated that the proposed model could represent the shear capacity of the test PCES beams reasonably, although it slightly underestimates the shear capacity. As can be seen from Table 3, the predicted shear capacities using the JGJ 138-2016 model are relatively conservative for the specimens, and the simplified calculation method can be also applied in preliminary design because of its convenience. Although the calculation method in the code YB 9082-2006 was also acceptable, some shear capacities of the test PCES beams were overestimated obviously, which might lead to potential risk in practical applications.

6. Conclusions

An innovative precast concrete-encased steel beam was proposed in this paper, and the shear performance of the proposed PCES beams under sagging moment and hogging moment was investigated. Based on the test observations and discussions of the experimental results, the following conclusions can be drawn:

- Due to the good behavior of the precast concrete transverse diaphragms, no obvious slippage was observed between the precast concrete and the cast-in-place concrete.

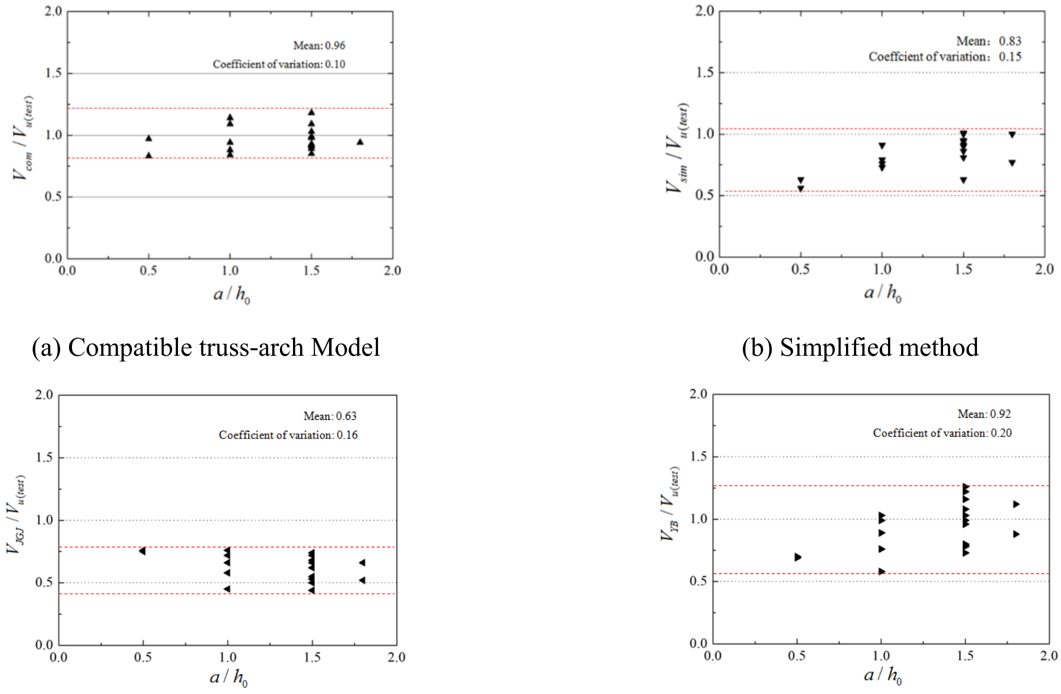

(a) Compatible truss-arch Model

(b) Simplified method

(c) Method in JGJ 138-2016

(d) Method in YB 9082-2006

Fig. 16 Variation of measured to calculated strength ratio versus shear span-to-depth ratio

All the specimens both under sagging moment and hogging moment failed in the typical shear compression mode. Attributed to the steel shape, the shear failure of the PCES beams was much more ductile than that of the traditional reinforced concrete beams.

- The shear capacity of the PCES beams was directly affected by the shear span-to-depth ratio, and the shear capacity decreased proportionally to the increasing of the shear span-to-depth ratio. Meanwhile, the existence of the concrete flange could increase the shear capacity of the entire PCES beam.
- Based on the deformation compatibility, a theoretical model for predicting the shear capacity of the PCES beams was proposed and verified to be valid with the good agreement of the shear capacities calculated using the proposed methods and those from the experiments. Then, a simplified calculation method for predicting the shear capacity of the proposed PCES beams based on the current design codes was also put forward and validated using the existing test results.

Acknowledgements

The experiments were sponsored by the National Natural Science Foundation of China (Grant No.51908450 and No. 51778525), and the Research Program of Key Labs affiliated to the Department of Education of Shaanxi Province (Grant No. 20JS068 and No. 2020PT-038). The financial support is highly appreciated.

References

Bentz, E.C., Vecchio, F.J. and Collins, M.P. (2006), “Simplified modified compression field theory for calculating shear strength of reinforced concrete elements”, *ACI Struct. J.*, **103**(4), 614-624.

Chen, Z. and Liu, X. (2018), “Seismic behavior of steel reinforced concrete cross-shaped column under combined torsion”, *Steel Compos. Struct.*, **26**(4), 407-420. https://doi.org/10.12989/scs.2018.26.4.407.

Choi, K.K. and Hong, G.P. (2007), “Unified shear strength model for reinforced concrete beams-Part II: verification and simplified method”, *ACI Struct. J.*, **104**(2), 153-161.

Collins, M.P., Mitchell, D., Adebar, P. and Vecchio, F.J. (1996), “A general shear design method”, *ACI Struct. J.*, **93**(1), 36-45.

Du, Y., Xiong, M.X., Zhu, J. and Liew, J.R. (2019), “Compressive and flexural behaviors of ultra-high strength concrete encased steel members”, *Steel Compos. Struct.*, **33**(6), 849-864. https://doi.org/10.12989/scs.2019.33.6.849.

Hong, W.K., Kim, J.M., Park, S.C., Kim, S.I., Lee, S.G., Lee, H.C. and Yoon, K.J. (2009), “Composite beam composed of steel and pre-cast concrete.(Modularized Hybrid System, MHS) Part II: analytical investigation”, *Struct. Des. Tall Spec. Build.*, **18**(8), 891-905. https://doi.org/10.1002/tal.484.

Hong, W.K., Park, S.C., Kim, J.M., Lee, S.G., Kim, S.I. and Yoon, K.J. and Lee, H.C. (2010a), “Composite beam composed of steel and precast concrete. (Modularized Hybrid System, MHS). Part I: experimental investigation”, *Struct. Des. Tall Spec. Build.*, **19**, 275-289. https://doi.org/10.1002/tal.507.

Hong, W.K., Park, S.C., Lee, H.C., Kim, J.M., Kim, S.I., Lee, S. G. and Yoon, K.J. (2010b), “Composite beam composed of steel and precast concrete (Modularized Hybrid System). Part III: Application for a 19-storey building”, *Struct. Des. Tall Spec. Build.*, **19**(6), 679-706. https://doi.org/10.1002/tal.507.

Hong, W.K., Kim, S.I., Park, S.C., Kim, J.M., Lee, S.G., Yoon, K. J. and Kim, S.K. (2010c), "Composite beam composed of steel and precast concrete (Modularized Hybrid System). Part IV: Application for multi-residential housing", *Struct. Des. Tall Spec. Build.*, **19**(7), 707-727. https://doi.org/10.1002/tal.506.

JGJ 138-2016 (2016), Code for design of composite structures, MoHURD; Beijing, China. (in Chinese)

Lacki, P., Derlatka, A. and Kasza, P. (2018), "Comparison of steel-concrete composite column and steel column", *Compos. Struct.*, **202**, 82-88. https://doi.org/10.1016/j.compstruct.2017.11.055.

Lai, B., Liew, J.Y. and Xiong, M. (2019), "Experimental and analytical investigation of composite columns made of high strength steel and high strength concrete", *Steel Compos. Struct.*, **33**(1), 67-79. https://doi.org/10.12989/scs.2019.33.1.067.

Li, X., Zhou, X., Liu, J. and Wang, X. (2019), "Shear behavior of short square tubed steel reinforced concrete columns with high-strength concrete", *Steel Compos. Struct.*, **32**(3), 411-422. https://doi.org/10.12989/scs.2019.32.3.411.

Kim, J.H. and Mander, J.B. (2007), "Influence of transverse reinforcement on elastic shear stiffness of cracked concrete elements", *Eng. Struct.*, **29**(8), 1798-1807. https://doi.org/10.1016/j.engstruct.2006.10.001.

Pan, Z.F. and Li, B. (2013), "Truss-Arch model for shear strength of shear-critical reinforced concrete columns", *J. Struct. Eng.*, **139**(4), 548-560. https://doi.org/10.1061/(ASCE)ST.1943-541X.0000677.

Patel, V.I., Uy, B., Pathirana, S.W., Wood, S., Singh, M. and Trang, B.T. (2018), "Finite element analysis of demountable steel-concrete composite beams under static loading", *Adv. Steel Constr.*, **14**(3), 392-411.

Placas, A. and Regan, P.E. (1971), "Shear failure of reinforced concrete beams", *Eng. Struct.*, **9**(87), 32-38.

Thusoo, S., Kono, S., Hamada, J. and Asai, Y. (2020), "Performance of precast hollow steel-encased high-strength concrete piles", *Eng. Struct.*, **204**, 109995.

Yan, B., Gan, D., Zhou, X. and Zhu, W. (2019). "Influence of slenderness on axially loaded square tubed steel-reinforced concrete columns", *Steel Compos. Struct.*, **33**(3), 375-388. https://doi.org/10.12989/scs.2019.33.3.375.

Yang, Y., Xue, Y. and Yu, Y. (2019a), "Theoretical and experimental study on shear strength of precast steel reinforced concrete beam", *Steel Compos. Struct.*, **32**(4), 443-454. https://doi.org/10.12989/scs.2019.32.4.443.

Yang, Y., Xue, Y., Yu, Y. and Gong, Z. (2019b), "Post-fire test of precast steel reinforced concrete stub columns under eccentric compression", *Steel Compos. Struct.*, **33**(1), 111-122. https://doi.org/10.12989/scs.2019.33.1.111.

YB 9082-2006 (2006), Technical Specification of Steel-Reinforced Concrete Structures, NDaRC; Beijing, China. (in Chinese)

Yu, Y. (2017), "Study on mechanical performance and design method on partially precast steel reinforced concrete beams", Ph.D. Dissertation, Xi'an University of Architecture and Technology, Xi'an. (in Chinese)

Zhu, W., Jia, J. and Zhang, J. (2017), "Experimental research on seismic behavior of steel reinforced high-strength concrete short columns", *Steel Compos. Struct.*, **25**(5), 603-615. https://doi.org/10.12989/scs.2017.22.5.603.

DL